14 Surface Physics

T. Greber, M. Hengsberger, J. H. Dil, H. Yanagisawa, H. Ma, R. Westerstrøm, L. Castiglioni, M. Morscher, F. Meier, D. Leuenberger, B. Slomski, S. Roth, H. Cun, A. Hemmi, G. Landolt, M. Greif, C. Janssen, P. Donà, S. Muff, L. Pazeller, M. Klöckner, J. Osterwalder

The group investigates surface and interface phenomena at the atomic level. For this purpose the surface physics laboratory is well equipped for the preparation and characterization of clean single-crystalline surfaces, metal and molecular monolayer films, as well as covalently bonded single layers, using a wide variety of experimental techniques. In addition, we currently operate two photoemission spectrometers at the nearby Swiss Light Source (SLS), one for spin- and angle-resolved photoemission spectroscopy (SARPES) and one for photoelectron diffraction and holography. Moreover, the group is participating actively in the buildup of the new beamline PEARL (PhotoEmission and Atomic Resolution Laboratory) at the SLS.

The research carried out during the report period can be grouped into four topics:

- **Monolayer films of hexagonal boron nitride (*h*-BN) and graphene on metal surfaces**
  Due to their strong intra-layer sp^2 bonds, these two materials form robust and chemically inert single honeycomb layers that couple weakly to the third dimension. The mechanical stiffness of these bonds leads to the formation of strongly corrugated superstructures with interesting functionalities when grown on top of transition metal surfaces with different lattice constants [1–3]. A prominent example is the boron nitride nanomesh that forms upon high-temperature chemical vapor deposition of borazine on Rh(111) [4]. Graphene forms corresponding structures on Rh(111) and Ru(0001) but with inverted corrugations [5]. These systems are studied in our group within two different contexts. The first one is the synthesis of heteroepitaxial layers of graphene and *h*-BN with a view on future electronic devices based on graphene. Due to its insulating properties and similar crystal structure and lattice constant, *h*-BN appears to be the ideal "gate oxide" [6]. The second context is the exploitation of these corrugated functional layers as templates for the growth of molecular adlayers with defined periodicities. Due to the inertness of these films, they can be brought into water or organic solvents, and we currently explore whether well-organized molecular layers can be deposited directly and much cheaper from solutions. This activity is supported by a Sinergia project of the Swiss National Science Foundation, funding a consortium of four different groups. Because these studies require a large supply of samples, a growth chamber has been built in which *h*-BN or graphene films can be grown on four-inch Si(111) wafers covered with monocrystalline Rh(111) films. The chamber is placed in a dedicated clean-room, which enables us to process these samples in a dust-free environment.

- **Molecular adsorbates and molecular monolayers**
  During this year we have continued to study the assembly of water molecules to small clusters when adsorbed at low temperature on the *h*-BN nanomesh. While coverages near one monolayer lead to the formation of nano-ice clusters of typically 40 atoms [7], water hexamers are the most frequent species at much lower coverages. These clusters are trapped by the ring dipoles surrounding the 2 nm wide pores of the nanomesh [3]. Exploratory studies of the adsorption of tetrafluoro-tetracyanoquinodimethane (TCNQF4), a molecule with a high electron affinity, on the nanomesh were carried out with the goal to observe the behaviour of a negatively charged species within the electrostatic landscape of the nanomesh. In a multilayer of

$Ar@C_{60}$ endofullerenes, the hybridization of the Ar 3p electronic level with molecular orbitals of the fullerene cage could be observed for the first time [8]. Finally, resonant x-ray photoelectron diffraction (RXPD) experiments have been performed with circularly polarized light of the SLS in order to combine structural information with sensitivity to magnetism. While this method will in the future be applied to magnetic molecules in order to study their magnetic coupling to a ferromagnetic substrate, a first proof-of-principle experiment has been carried out on a clean Ni(111) sample (see Sec. 14.1).

- **Ultrafast processes at surfaces**
  This past year marks the start of the new NCCR 'Molecular Ultrafast Science and Technology' (MUST) in which our group participates with an activity aimed at femto- and attosecond studies of molecular processes at surfaces. In the first project year a compact angle-resolved photoemission chamber was designed and ordered, which will be moved to various ultrashort pulsed light sources available within the consortium. Concurrently, the existing photoemission chamber equipped with an elliptical display analyzer (EDA) was used to study Bi(114), a stepped surface where strong spin-orbit splitting leads to a spin-split one-dimensional surface state [9]. In a parallel activity, the photo-induced field emission spectra resulting from focussing a pulsed laser beam tightly onto a sharp tungsten tip could be understood quantitatively (see Sec. 14.3).

- **Spin-resolved photoemission and momentum mapping**
  Our spin-resolved photoemission chamber (COPHEE) at the SLS has continued to be in high demand as a general user instrument due to its unique performance. Spectacular results were obtained in collaboration with a group from Princeton University on a novel class of materials, so-called *topological insulators*. Spin-resolved ARPES data measured at the COPHEE end station have helped to demonstrate the spin texture inversion below and above the Dirac point in $BiTlSe_2$ [10] (see Sec. 14.2). In the meantime the group has started its own, independent activity on topological insulators, focusing on the growth of ultrathin films and on new compounds. Moreover, the studies of the Rashba effect in ultrathin Pb films on Si(111) were continued with the goal to influence the spin splitting of the quantum well states by interface engineering. A strong dependence of the electron effective mass of these states on the character of the interface could be explained [11]. Finally, spin state interference was observed in the surface alloy of Sb/Ag(111), a system where the Rashba-type spin splitting of the surface states is smaller than the intrinsic linewidth of their photoemission peaks. As a consequence, the spin polarization vector rotates into the plane perpendicular to the quantization axis of the Rashba system [12].

In the following, three highlights of last year's research are presented in more detail.

[1] T. Greber, e-J. Surf. Sci. Nanotechnol. 8, 62 (2010).

[2] S. Berner *et al.*, Angew. Chem. Int. Ed. 46, 5115 (2007).

[3] J. H. Dil *et al.*, Science 319, 1824 (2008).

[4] M. Corso *et al.*, Science 303, 217 (2004).

[5] T. Brugger *et al.*, Phys. Rev. B 79, 045407 (2009).

[6] C. R. Dean *et al.*, Nature Nanotech. 5, 722 (2010).

[7] H. Ma *et al.*, Chem. Phys. Chem. 11, 399-403 (2010).

[8] M. Morscher *et al.*, Phys. Rev. A 82, 051201(R) (2010).

[9] J. W. Wells *et al.*, Phys. Rev. Lett. 102, 096802 (2009).

[10] Su-Yang Xu *et al.*, ScienceExpress, DOI: 10.1126/science.1201607.

[11] B. Slomski *et al.*, Phys. Rev. B 83, 035409 (2011).

[12] F. Meier *et al.*, J. Phys: Condens. Matter 23, 072207 (2011).

14.1 Resonant photoelectron diffraction (RXPD) for the determination of magnetic and atomic structure

in collaboration with: Frithjof Nolting, Swiss Light Source, PSI, CH-5232 Villigen, Switzerland.

X-ray photoelectron spectroscopy (XPS) with angular resolution (XPD) allows structure determination paired with chemical and magnetic sensitivity [1]. At x-ray absorption resonance the signal is maximal for a given chemical species [2; 3]. If resonant angle scanned photoelectron diffraction (RXPD) is applied to a magnetic system the magnetization direction can be extracted from the dichroic signature in the x-ray absorption coefficient, which depends on the orientation of the angular momenta of the exciting photons with respect to the magnetisation. For magnetized Ni(111) the XPD patterns excited with circularly polarized light at the L_2 resonance yield the precise structure and magnetization direction [4].

Figure 14.1 shows the circular dichroism in the photoemission spectra which are excited at the L_2 ($2p_{\frac{1}{2}} \rightarrow 3d$) x-ray absorption resonance ($\hbar\omega = 870.5$ eV) with right (σ^+) and left (σ^-) circularly polarized photons. In ferromagnetic nickel the 3d valence shell is spin polarized, which produces a pronounced dichroism. Figure 14.2 displays XPD patterns of Ni(111). The XPD map in (a) is dominated by the information on the atomic structure which corresponds to that of a face centered cubic (fcc) crystal that is cut along the (111) plane [5]. In order to visualize the dichroic information, we form the asymmetry between the α_2^+ and the α_2^-

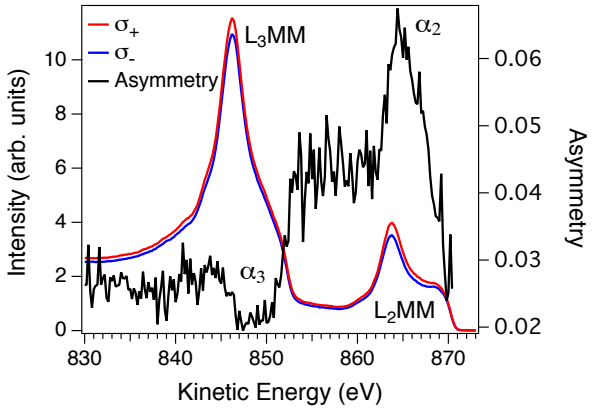

Fig. 14.1 – Near normal photoemission spectra from magnetized Ni(111) excited with left and right circularly polarized light (σ^+ and σ^-). The photon energy was set to the L_2-resonance at $\hbar\omega = 870.5$ eV. The spectra have been normalized with the photon flux. The L_2MM and the L_3MM Auger deexcitation peaks are indicated. The asymmetry between right and left circularly polarized light exhibits two distinct extrema α_2 and α_3, on which we performed XPD measurements.

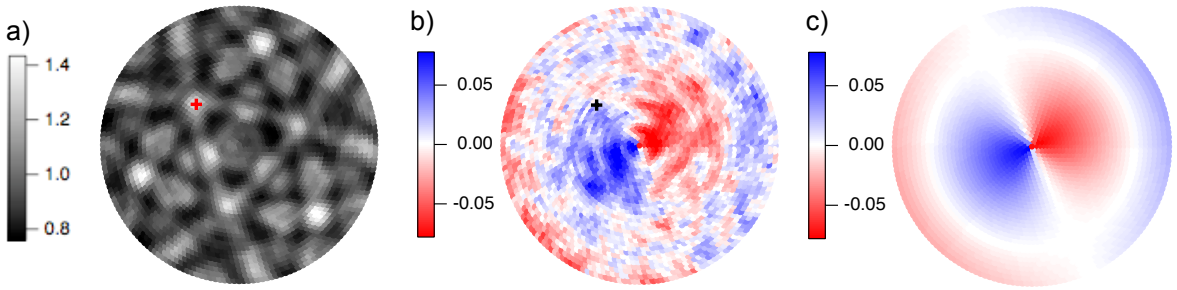

Fig. 14.2 – (a) Resonant x-ray photoelectron diffraction (RXPD) data of Ni(111). The 3500 stereographically projected data points for polar angles $0 \leq \theta \leq 70°$ of the intensity at α_2 (E_{kin}=863.8 eV, $\hbar\omega = 870.5$ eV, σ^+) in Fig. 14.1. The data are normalized with the average polar intensity. The [011]-direction is marked with a red cross. (b) Asymmetry of two XPD data sets at α_2 measured with right and left circularly polarized light. The twofold i.e. dipolar pattern reveals the direction of the magnetization. (c) Fit of the dichroic dipole (D-function) to the asymmetry in (b).

XPD scans (see Fig. 14.2b). These data contain information on the dipolar (magnetic) nature of dichroism and higher order multipoles, which are related to differences in the diffraction patterns due to different source waves [6; 7]. The dipolar part has the symmetry expected for in plane magnetisation. Figure 14.2c shows the fit of a dipolar function D, which determines the direction of the average magnetisation $\mathbf{m}'$. The rotation of the sample and the incidence of the light impose on D *two* nodal lines ($\mathbf{m}' \cdot \mathbf{L}_{ph} = 0$), where $\mathbf{L_{ph}}$ is the angular momentum vector of the photons.

These experiments show that resonant photoelectron diffraction may be exploited in the study of the geometric structure around a photoemitter and its magnetic momentum orientation [4]. We expect the method to be useful for the investigation of the spin structure in magnetic molecules.

[1] C. S. Fadley, J. Electron Spectrosc. Relat.Phenom. 78, 2 (2010).

[2] P. Krüger *et al.*, Phys. Rev. Lett. 100, 055501 (2008).

[3] M. Treier *et al.*, Phys. Rev. B 80, 081403 (2009).

[4] M. Morscher *et al.*, arXiv:1103.4280.

[5] J. Wider *et al.*, Phys. Rev. Lett. 86, 2237 (2001).

[6] T. Greber *et al.*, Phys. Rev. B 45, 4540 (1992).

[7] H. Daimon *et al.*, Jap. J. Appl. Phys. 32, L1480 (1993).

14.2 Symmetry protected spin structures in topological insulators

in collaboration with: Zahid Hasan, Department of Physics, Princeton University, Princeton, New Jersey 08544, USA; and Luc Patthey, Swiss Light Source, Paul Scherrer Insititute, 5232 Villigen, Switzerland.

Topological insulators are a novel phase of condensed matter where strong spin-orbit interaction induces a band gap in the bulk but also the formation of topologically protected surface states [1]. This protection is caused by a peculiar spin structure of the surface states: for a given momentum direction there is only one (or in the extended case any other odd number) spin-polarized Fermi level crossing. Because time-reversal symmetry is not broken in these materials it follows that for opposite momenta the spin also has to be opposite. Therefore backscattering of non-magnetic defects is highly reduced as it would require a spin flip. A further concequence of the time-reversal symmetry is that the spin-polarized bands must cross at the centre of the Brillouin zone, where the momentum is zero, and at other specific high symmetry points linked by a reciprocal lattice vector. The odd number of spin-polarized bands and the forced crossing at given points in the Brillouin zone together guarantee that the surface states will always cross the Fermi level as long as time-reversal symmetry is not broken. This is in short what constitutes the topological protection of the surface metallicity.

The fact that the unusual properties of a topological insulator are determined by the spin structure of its surface states makes spin- and angle-resolved photoemission (SARPES) an central experimental probe for these systems [2]. In Fig. 14.3 the measured spin-polarization and resulting spin structures are shown for Bi_2Te_3. Through these measurements we could unambiguously verify that these systems are topological insulators with only a single Dirac cone at the surface [3]. However, it has been found that for Bi_2Te_3 the Dirac cone is not perfectly circular for energies away from the Dirac point, but becomes increasingly hexagonal and even snow-flake like [4]. As a concequence of

this warping it is expected that the spin polarization vector obtains an out-of-plane component between the cusps of the constant energy surfaces [5]. As can be seen in the spin-structure summary in Fig. 14.3 this is exactly what we observe for Bi_2Te_3 in our spin-resolved photoemission experiments.

The three-fold symmetry of the out-of-plane polarization significantly enhances the phase-space for scattering events and thus reduces the conductivity. On the other hand, it also increases the possibility for spin injection into the system and gives an extra degree of freedom for any spin manipulation. By using ternary instead of binary compounds the number of possible topological insulators, with potentially different electronic and spin texture properties, is dramatically enhanced. This is exemplified by the results obtained for $TlBiSe_2$ shown in Fig. 14.4. For this system the Dirac point is well separated from the bulk valence band which allows us to measure the spin texture below this crossing point [6]. As can be seen in Fig. 14.4b) the momentum scan measured below the Dirac point shown an inverted spin-polarization signal compared to all measurements performed above this point. This means that when one places the chemical potential at the Dirac point only a very small voltage needs to be applied to switch between reversed spin textures. This could thus be an interesting material for realizing a low-power spin transistor.

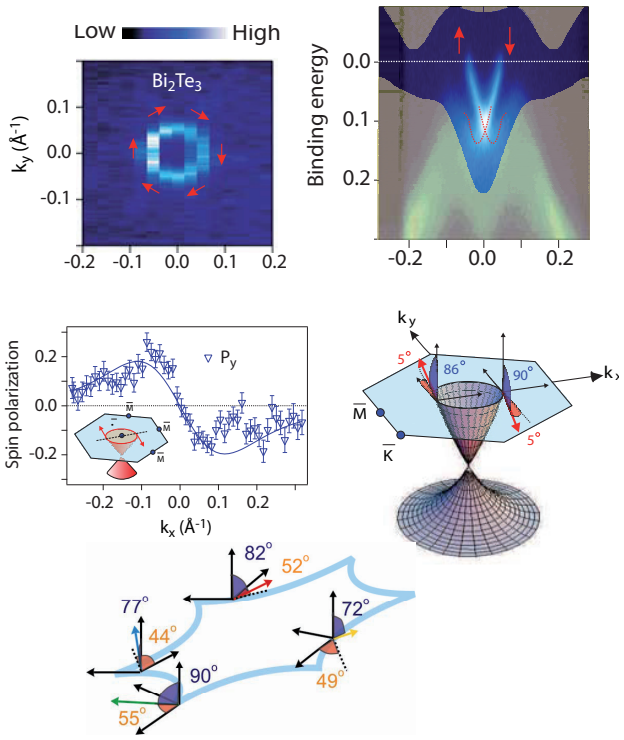

Fig. 14.3 – Experimental Fermi surface and band dispersion (top two panels), as well as spin texture (bottom three panels) of the single Dirac cone topological insulator Bi_2Te_3 (from Ref. [3]).

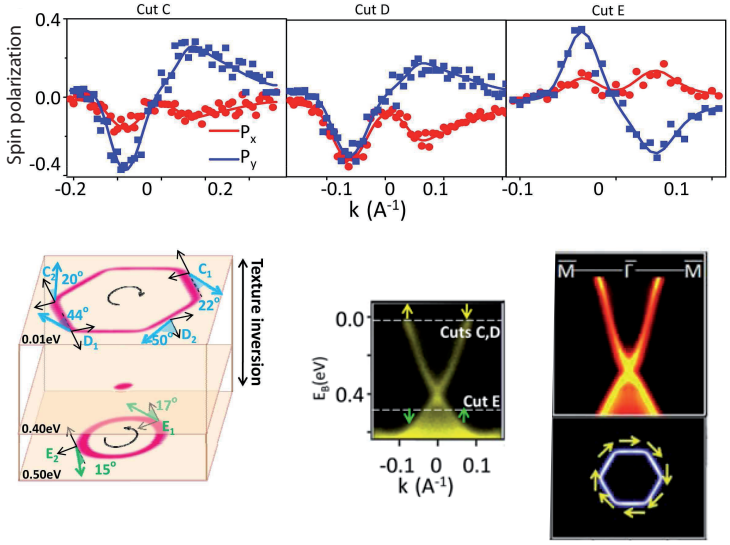

Fig. 14.4 – Dirac cone and spin structure of $TlBiSe_2$ showing the reversal of the spin texture above and below the Dirac point. Top panels: spin polarization curves along the cuts indicated in the center figure below. Bottom left: schematic illustration of constant energy surfaces observed at two energies, one above and one below the Dirac point. Spin polarization vectors measured at selected points are also plotted (from Ref. [6]).

[1] M. Z. Hasan and C. L. Kane, Rev. Mod. Phys. 82, 4 (2010).
[2] J. H. Dil, J. Phys.: Condens. Matter 21, 403001 (2009).
[3] D. Hsieh *et al.*, Nature 460, 1101 (2009).
[4] Z. Alpichshev *et al.*, Phys. Rev. Lett. 104, 016401 (2010).
[5] L. Fu, Phys. Rev. Lett. 103, 266801 (2009).
[6] Su-Yang Xu *et al.*, ScienceExpress, DOI: 10.1126/science.1201607.

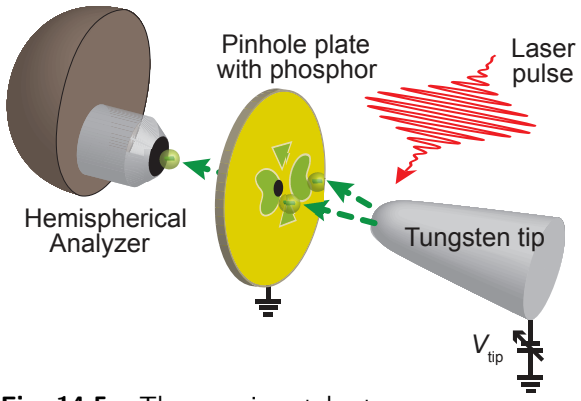

Fig. 14.5 – The experimental setup.

14.3 Ultrafast dynamics in photo-induced field emission

in collaboration with: Christian Hafner, Laboratory for Electromagnetic Fields and Microwave Electronics, ETH Zürich.

When a focused laser pulse illuminates a metallic tip, optical electric fields are enhanced at the tip apex due to plasmonic effects, and the enhanced fields induce pulsed field emission in combination with a moderate DC voltage applied to the tip. Depending on the strength of the enhanced fields, different field emission mechanisms are considered to be dominant [1; 2]. For relatively weak fields, single-electron excitations by single- and multi-photon absorption are prevalent, and photo-excited electrons are tunneling through the surface potential barrier; this so called photo-field emission process is most interesting for applications and was studied in our lab in great detail.

Previously it was found that two-photon photoemission yields the best compromise between a high multi-photon excitation cross section and a thin tunneling barrier [3]; this finding was obtained by simulating the local field enhancement by solving the Maxwell equations using finite-elements methods [4], and by calculating the local emission currents within Fowler-Nordheim theory. In order to confirm experimentally the relative contributions for various parameter sets (bias voltage, laser focus and intensity) we upgraded our field emission setup by implementing an electron energy analyzer (see Fig. 14.5). In order to distinguish electrons emitted from different facets of the tungsten tip, a large plate with phosphor coating and pinhole in the center was installed as a counter electrode between the tip and the analyzer. The field emission pattern of the clean tungsten tip can be observed on the phosphor plate where the most intense electron emission is observed around the [310]-type facets. The pinhole is positioned at the edge of one of those regions (see Fig. 14.5).

The field emission current is influenced by two factors: 1) the electron occupation number and 2) the transmission probability through the surface barrier [5; 6]. The occupation number is given by an electron distribution function $f(E)$, which is the Fermi-Dirac distribution function in the case of field emission, and the transmission probability depends exponentially on an area of the surface barrier indicated by the hatched area in Fig. 14.6a. Therefore, the positive energy side of the spectrum falls off due to a rapid decrease of the occupation number, while the negative energy side falls off because of the exponential decay of the transmission probability due to the increase of the surface barrier area. A typical field emission spectrum shows thus an asymmetric peak. An energy spread of 0.21 eV was observed, which is close to the value measured with 1 meV energy resolution in previous work (0.19 eV) [7], confirming our reasonable energy resolution.

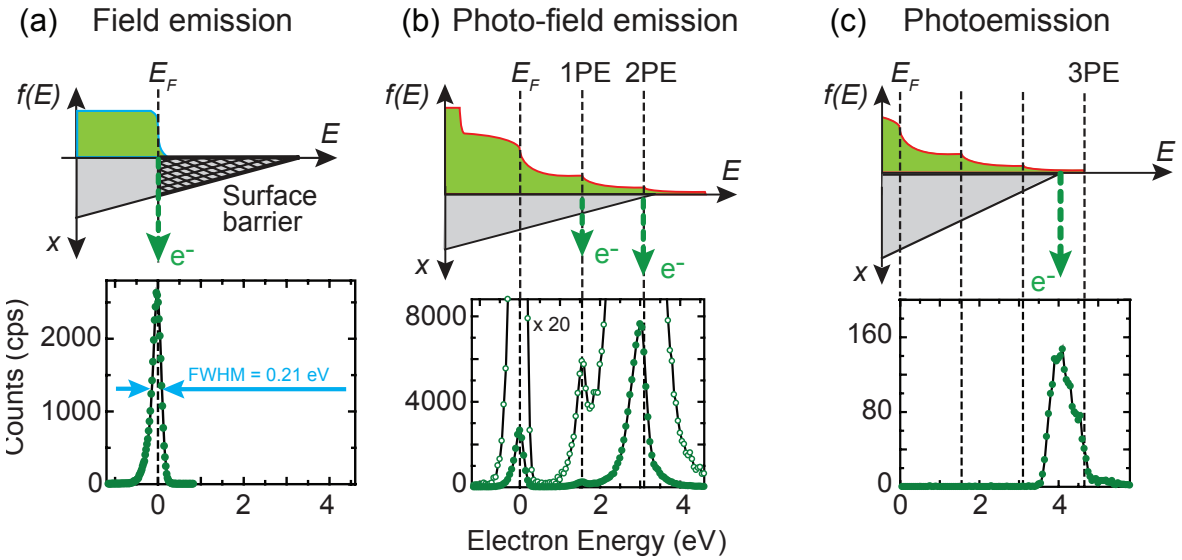

Fig. 14.6 – Top panels: schematic energy diagrams illustrating the different mechanisms that contribute to the electron yield. Bottom panels: measured energy distributions.
(a) Field emission from a Fermi-Dirac distribution. The tip voltage V_{tip} was -2300 V and no laser was used.
(b) Nonequiliburium electron distribution just after laser absorption including electron-electron scattering; V_{tip} = -2300 V and laser power P_L = 50 mW.
(c) At low bias voltage V_{tip} = -500 V and high laser power P_L = 50 mW 3-photon photoemission dominates.

When illuminated by a pulsed laser with moderate peak intensity, the current increases due to photoexcited carriers, which encounter a largely reduced tunneling barrier at higher energy. As conjectured in Ref. [3], the spectrum is dominated by electrons excited by two photons as shown in the spectrum in Fig. 14.6b. Eventually, as the bias voltage is reduced the tunneling barrier becomes too large and the emission spectrum is dominated by photoelectrons excited in a three-photon process as shown in spectrum (c). This is the first time that photon-field emission spectra were measured in such detail, and corroborated by full dynamical calculation including the electron-electron scattering dynamics and the transient heating of the electron gas. The results are published in a forthcoming paper [8].

At the end of 2010, H. Yanagisawa was awarded an *Ambizione* grant by the Swiss National Science Foundation. He has moved the setup to ETH Zürich, where he will continue this research using phase-controlled few-cycle laser pulses available in the laboratory of Prof. U. Keller.

[1] P. Hommelhoff *et al.*, Phys. Rev. Lett. 96, 077401 (2006).
[2] H. Yanagisawa *et al.*, Phys. Rev. Lett. 103, 257603 (2009).
[3] H. Yanagisawa *et al.*, Phys. Rev. B 81, 115429 (2010).
[4] For Max-1, see http://alphard.ethz.ch/.
[5] R. Gomer, "Field Emission and Field Ionization", (American Institute of Physics, New York, 1993).
[6] G. Fursey, "Field Emission in Vacuum Microelectronics", (Kluwer Academic / Plenum Publishers, New York, 2003).
[7] H. Ogawa *et al.*, Surf. Sci. 357-358, 371 (1996).
[8] H. Yanagisawa *et al.*, cond-mat: arXiv 1103.4310.